remote sensing

MDPI

Article

Hyperspectral Estimation of Leaf Nitrogen Content in White Radish Based on Feature Selection and Integrated Learning

Yafeng Li [1,2], Xingang Xu [1,2,*], Wenbiao Wu [1], Yaohui Zhu [2], Guijun Yang [1], Lutao Gao [3], Yang Meng [1], Xiangtai Jiang [1] and Hanyu Xue [1]

[1] Key Laboratory of Quantitative Remote Sensing in Ministry of Agriculture and Rural Affairs, Information Technology Research Center, Beijing Academy of Agricultural and Forestry Sciences, Beijing 100097, China; 2222216013@stmail.ujs.edu.cn (Y.L.); wuwb@nercita.org.cn (W.W.); yanggj@nercita.org.cn (G.Y.); mengy@nercita.org.cn (Y.M.); jiangxt@webmail.hzau.edu.cn (X.J.); 2222116047@stmail.ujs.edu.cn (H.X.)
[2] School of Agricultural Engineering, Jiangsu University, Zhenjiang 212013, China; yaohui_zhu@ujs.edu.cn
[3] College of Big Data, Yunnan Agricultural University, Kunming 650500, China; 2013015@ynanu.edu.cn
* Correspondence: xuxg@nercita.org.cn

Abstract: Nitrogen is the main nutrient element in the growth process of white radish, and accurate monitoring of radish leaf nitrogen content (LNC) is an important guide for precise fertilization decisions for radish in the field. Using white radish LNC monitoring as an object, research on radish nitrogen hyperspectral estimation methods was carried out based on leaf hyperspectral and field sample nitrogen data at multiple growth stages using feature selection and integrated learning algorithm models. First, the Vegetation Index (VI) was constructed from hyperspectral data. We extracted sensitive features of hyperspectral data and VI response to radish LNC based on Pearson's feature-selection approach. Second, a stacking-integrated learning approach is proposed using machine learning algorithms such as Support Vector Machine (SVM), Random Forest (RF), and Ridge and K-Nearest Neighbor (KNN) as the base model in the first layer of the architecture, and the Lasso algorithm as the meta-model in the second layer of the architecture, to realize the hyperspectral estimation of radish LNC. The analysis results show the following: (1) The sensitive bands of the radish LNC are mainly centered around 600–700 nm and 1950 nm, and the constructed sensitive VIs are also concentrated in this band range. (2) The Stacking model with spectral features as inputs achieved good prediction accuracy at the radish spectral leaf, with R^2 = 0.7, MAE = 0.16, MSE = 0.05 estimated over the whole growth stage of radish. (3) The Lasso algorithm with variable filtering function was chosen as the meta-model, which has a redundant model-selection effect on the base model and helps to improve the quality of the integrated learning framework. This study demonstrates the potential of the stacking-integrated learning method based on hyperspectral data for spectral estimation of nitrogen content in radish at multiple growth stages.

Keywords: LNC; leaf hyperspectral; vegetation index; feature selection; machine learning; stacking learning; lasso algorithm

check for updates

Citation: Li, Y.; Xu, X.; Wu, W.; Zhu, Y.; Yang, G.; Gao, L.; Meng, Y.; Jiang, X.; Xue, H. Hyperspectral Estimation of Leaf Nitrogen Content in White Radish Based on Feature Selection and Integrated Learning. *Remote Sens.* **2024**, *16*, 4479. https://doi.org/10.3390/rs16234479

Academic Editor: Lenio Soares Galvao

Received: 12 October 2024
Revised: 26 November 2024
Accepted: 26 November 2024
Published: 29 November 2024

Copyright: © 2024 by the authors. Licensee MDPI, Basel, Switzerland. This article is an open access article distributed under the terms and conditions of the Creative Commons Attribution (CC BY) license (https://creativecommons.org/licenses/by/4.0/).

1. Introduction

Radish is a major cultivated crop in China with a wide range of dietary and therapeutic applications. Nitrogen is the main nutrient element in the growth process of radish, which has an important influence on the formation of the final yield and quality of radish [1,2]. Nitrogen deficiency causes slow growth and reduces the nutrient content of radishes [3]. In production, the excessive pursuit of high yield has promoted the increase of crop yield, but the excessive application of nitrogen fertilizer has caused a huge waste of agricultural resources while bringing about serious farmland ecological environment problems [4,5]. According to the characteristics of the growth and development of different crops, accurate, rapid and timely monitoring of crop nutrients is the basis of rational fertilization [6]. Traditional LNC calculations are based on destructive field sampling and laboratory analysis,

resulting in inefficiencies that are not applicable to real-time monitoring over large areas and multiple crop cycles [7]. Remote sensing technology, as an efficient and non-destructive monitoring technology that can be easily applied over large areas, is widely used for precision agriculture crop monitoring. These include monitoring of biological variables [8], monitoring of plant pests and diseases [9], and yield prediction [10].

Hyperspectral data are uniquely suited to detecting detailed spectral changes in plant stress response due to their rich band information and sensitivity to vegetation changes [11]. It has been shown that using the absorption differences and reflectance properties of crops in different bands to construct vegetation indices to predict LNC can achieve good results [12,13]. Lu et al. extracted four vegetation indices such as green–red ratio (GRRI) in the visible spectrum to estimate summer maize LNC (R^2 = 0.758, RMSE = 0.147%) [14]. Yang et al. searched for LNC-sensitive vegetation indices by hyperspectral reflectance of grape leaves and constructed a prediction model, and proposed three vegetation indices calculated by first-order derivatives of the bands with good prediction results [15]. However, the VI ignores a great deal of spectral information and suffers from a lack of generalizability in the model. The integrated learning model performs stably in dealing with noise and outliers, and therefore full-band hyperspectral data are more suitable for assessing vegetation traits than vegetation indices in this model. The ability to retrieve crop nutrients from in situ hyperspectral data has also been demonstrated [16,17]. Tan et al. analyzed the quantitative relationship between rice canopy hyperspectral data and nitrogen content, screened the sensitive bands and performed regression prediction based on binary particle swarm (BPSO) and support vector machine (SVM), and found that a strong fit was achieved at the three selected growth stages [18]. Thorp et al. used a genetic algorithm (GA) for wheat nitrogen status estimation by extracting relevant information from full-spectrum data [19]. Guo et al. extracted feature bands for predicting rubber tree LNC using Competitive Adaptive Reweighted Sampling–Successive Projections Algorithm (CARS-SPA) [20]. Therefore, the use of in situ hyperspectral data combined with integrated learning models can provide an efficient and accurate method for predicting the LNC of radishes.

High-dimensional hyperspectral data contains hundreds of bands, some of which are highly correlated with each other. This leads to an increase in the redundancy of spectral information, which reduces the computational speed and leads to a decrease in the inversion accuracy [21,22]. How to improve the computational efficiency of the model and simplify the model structure while maximizing the retention of spectral information through feature filtering is crucial [23]. Pearson correlation analysis is a more commonly used method for calculating correlation coefficients, which is widely used to assess the correlation between hyperspectral data and physiological and biochemical parameters, such as LNC [24] and leaf chlorophyll content (LCC) [25]. Various machine learning models have been used for prediction of vegetation physiological parameters and have shown good potential in monitoring LNC [26,27]. However, different machine learning models have different data requirements, the canopy and leaf structure of radish is significantly different from that of traditional food crops. Integration learning allows for the integration of various model results, which can reduce prediction errors and improve prediction accuracy and model generalization capabilities [28,29]. Xiao et al. estimated citrus LCC based on leaf hyperspectral data by combining the integrated learning regression model with fractional order differentiation (FOD) and wavelet transform (CWT) spectral processing methods [30]. Huang et al. established a hybrid method to estimate LCC based on three band-selection methods (RFE, CA, VIP), an integration algorithm and PROSAIL modeling [31]. Multiple studies have shown good results of integrated learning models in monitoring physiological and biochemical parameters of different crops.

Integrated learning predictive models include bagging, stacking, and LightGBM. Stacking can give full play to the characteristics and advantages of the base model, and the choice of the base model is relatively flexible, which can be adapted to different types of data and problems. In order to improve the generalization performance and estimation

accuracy of the white radish LNC estimation model, this paper uses the stacking-integrated learning regression model to estimate radish LNC.

An excessive number of base models increases the model complexity and computational cost, and previous studies usually chose linear models in the selection of meta-models [32]. This means that only the base model results are used as inputs to the meta-model, ignoring the performance of the base model. When the base model does not work well, simple stacking creates redundancy and the meta-modeling results are compromised. Lasso regression introduces the L1 paradigm as a regularization term based on the traditional linear regression model, and the greater regularization strength forces the weight coefficients of unimportant features to converge to zero, facilitating feature selection [33,34]. That is, when we use Lasso regression as a meta-model, the poorly performing base model will have a weight of 0, which will further improve the model's explanatory and generalization capabilities.

In this paper, based on leaf hyperspectral data of radish at three major growth stages and constructing vegetation indices, combined with the Pearson algorithm to calculate the importance of characteristic variables, an integrated learning regression model with Lasso regression model as a meta-model was proposed to predict radish LNC. The specific contributions of this study are as follows:

(1) Radish leaf hyperspectral (350–2500 nm) and LNC data were collected and measured, and 20 typical VIs were constructed. Sensitive features were screened by Person's calculation of the correlation coefficients of spectra in each band and VIs to LNC.
(2) In order to further validate the processing capability of stacking on high-dimensional input features, we built hyperspectral-stacking and VI-stacking radish LNC prediction models with multiple growth stages for comparative analysis.
(3) We discuss the accuracy of the proposed method for LNC prediction at different growth stages of radish.

2. Materials and Methods

2.1. Study Area

The experimental area is located in Shiping County, Honghe Hani, and Yi Autonomous Region, Yunnan Province, China, with an average annual temperature of 18.3 °C and annual precipitation ranging from 786 to 1116 mm. Due to the unique climate and soil conditions, which provide a suitable environment for the growth of white radish, it has become a leading industry for local growers to increase their income. "Harvesting more or less lies in the fertilizer", nitrogen as an important mineral element required for radish growth, accurate real-time monitoring of LNC, for the realization of accurate fertilization-management decisions in farmland, to enhance the yield while increasing the utilization rate of fertilizers, and is of great significance to the promotion of sustainable development of agriculture.

Figure 1 shows the study area of this paper, which consists of 27 plots, each with a planting area of 6 m × 10 m. The following fertilization treatments were applied to 18 plots: 2.43 kg (N1), 2.025 kg (N2), 1.62 kg (N3), 1.215 kg (N4), 0.81 kg (N5), 0.405 kg (N6). The rest of the plots were controls (N0), and each group of nitrogen treatments was replicated three times, using a mixture of nitrogen, phosphorus, and potassium at a ratio of 23:13:6 for type of fertilizer for fertilization treatments. The study collected data from three major radish reproductive stages: rosette stage (4 November 2023), fleshy root growth bloom (29 November 2023; 20 December 2023), and maturity stage (10 January 2024). As shown in Figure 1, for each growth stage, a group of nitrogen treatments and four controls (10 sample points) were selected as the validation data for each growth stage, and the rest of the data were divided into training and testing sets in a 7:3 manner to establish the LNC prediction model for all the growth stages (17 × 4 sample points).

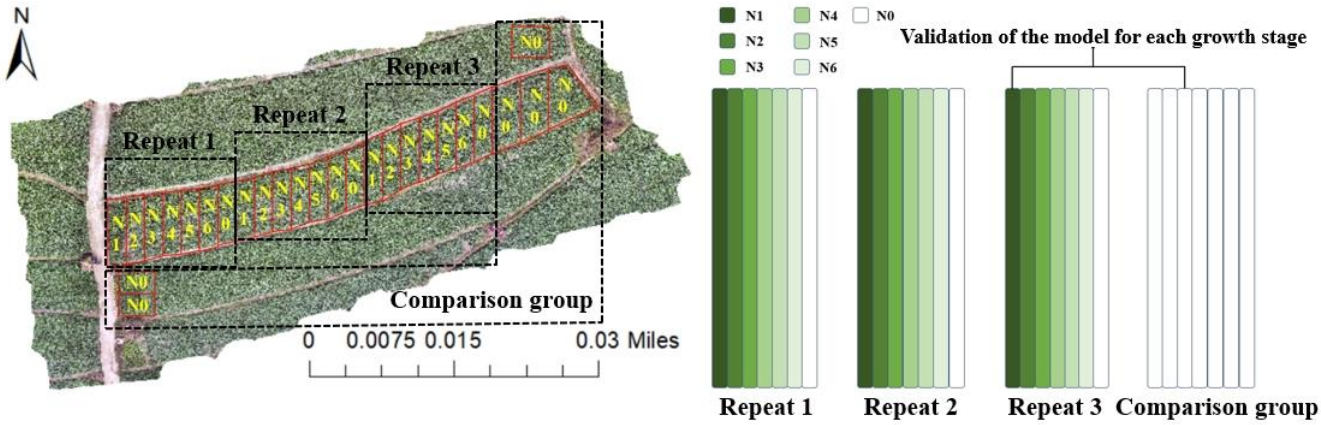


Figure 1. Study area and nitrogen treatment.

2.2. Ground Data Acquisition and Radish LNC Determination

Two radishes were selected as specimens for each plot, and the spectral reflectance of the test samples was determined using an American ASD Field Spec Pro 2500 back-mounted field spectrometer with a detection range of 350–2500 nm in the spectral bands, and the band accuracy and spectral resolution were adjusted to 1 nm. Leaf spectral determination was carried out indoors using the instrument's built-in light source, after stem and leaf separation of the specimen, 10 leaves with uniform growth were selected as the standard leaves, and the leaves were flattened and placed under the spectral detector for determination, the leaf veins were avoided during the collection, and one spectral reflectance was collected from each leaf and then averaged as the leaf spectra of the plot. After spectral collection, the labeled leaves were placed in paper bags in an oven at 105 °C for 0.5 h, and then the leaf samples were dried at 80 °C for more than 48 h until the mass was determined. All dry leaf samples were then weighed and ground and pulverized, and nitrogen concentration was measured by the Kjeldahl method. The LNC unit is g/100 g and we abbreviate the unit as %.

The acquired data are shown in Figure 2, representing the hyperspectral transformation curves of radish leaves at different growth stages and the trend of LNC changes. The radish growth cycle includes the germination stage, seedling stage, pre-flesh root growth (rosette stage), late fleshy root growth, and maturity stage. This study focuses on analyzing data from the last three critical growth stages. Leaf growth is vigorous during the rosette stage, during which the number of leaves is increasing, leaf area is expanding rapidly, and fleshy root lengthening and thickening growth are occurring simultaneously, taking 20–30 days. Above-ground growth exceeded below-ground growth, and the absorbed nitrogen was mainly supplied to leaf growth, so leaf LNC was highest at this growth stage. The fleshy roots continued to mature during the later stages of fleshy root growth, which took 40–45 days, and data were collected twice during this reproductive period. This is the period of the fastest growth of fleshy roots and the period where the aboveground growth is gradually slowed down and a large number of assimilated products are transported to the fleshy roots for storage and accumulation, resulting in rapid growth of fleshy roots and lower LNC. After the formation of fleshy roots, the crop enters the maturity stage and gradually stops growing during this reproductive stage due to the turning of the climate. LNC was above 4% at all three reproductive stages, and was highest at the rosette stage when aboveground growth was predominant. LNC declined rapidly during the fleshy root growth stage and rose slowly with lower growth.

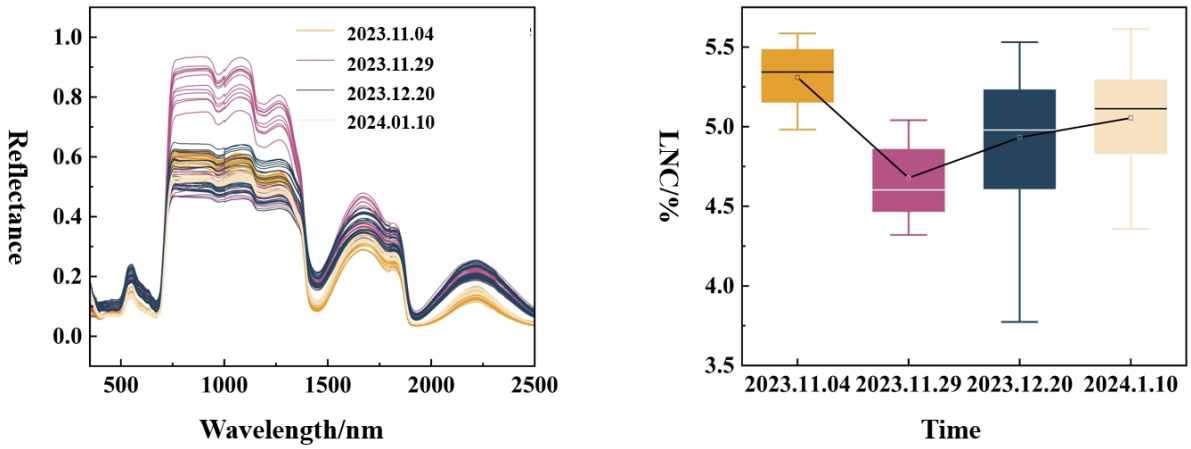


Figure 2. Hyperspectral and LNC of radish leaves at different growth stages.

2.3. Methods

Figure 3 shows the stack-integrated learning architecture of the study, the detailed parts of which are as follows:

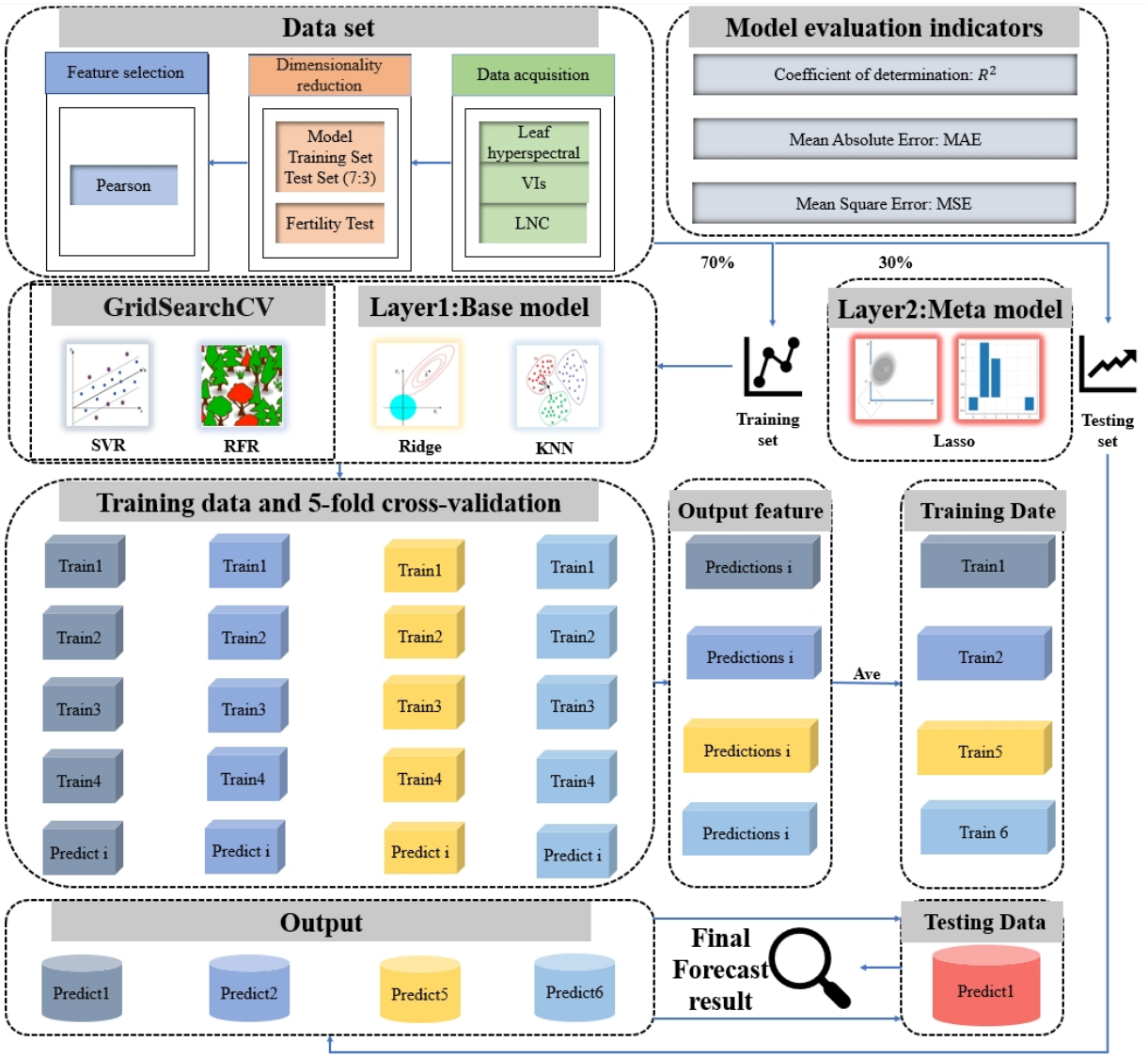


Figure 3. Stack-integrated learning architecture.

Data collection and segmentation: Hyperspectral data (350–2500 nm) of radish leaves were measured using ASD and typical VIs were constructed. The LNC of the samples was measured using the Kjeldahl method. Each growth stage consisted of 27 plots (3 sets of nitrogen replicates and 9 controls), and one set of nitrogen replicates and 4 controls were taken to validate the model data for the crop growth stage. The rest of the data consisted of 17 × 4 (two nitrogen replicates, 5 controls, 4 periods of data), totaling 68 sample points, which were subjected to randomized disorder processing and then divided into 7:3 training and test sets for training and analysis of the stacking model.

Feature selection: the ability of each band to characterize the LNC with VI was calculated using the Pearson feature-selection algorithm (full life span). Pearson's correlation coefficient provides a quick understanding of the linear correlation between the features and the corresponding variables, and is directional, with an output ranging from −1 to +1. It can be a measure of the strength of the relationship between the variables—the closer to 0, the lower the correlation—and is a special type of covariance that is standardized by removing the effect of the magnitude of the variables on both sides [35,36]. Once the correlation coefficient has been calculated, the strength of the correlation of the variables can be determined by the following ranges of values: 0–0.2 (very weak correlation), 0.2–0.4 (weak correlation), 0.4–0.6 (moderate correlation), 0.6–0.8 (strong correlation), and 0.8–1 (very strong correlation). In this study, correlation coefficients of 0.6 or higher were used as feature-selection criteria. The formula is as follows:

$$r = \frac{\sum_{i=1}^{n} \left(X_i - \overline{X}\right)\left(Y_i - \overline{Y}\right)}{\sqrt{\sum_{i=1}^{n} \left(X_i - \overline{X}\right)^2} \sqrt{\sum_{i=1}^{n} \left(Y_i - \overline{Y}\right)^2}} \quad (1)$$

where X_i denotes reflectance, Y denotes LNC, and n denotes sample point, $i = 1, 2, \ldots, n$.

Model construction: sensitive bands and typical VIs are used as model inputs, Support Vector Machine (SVM), Random Forest (RF), Ridge, and K-Nearest Neighbor (KNN) algorithms are used as base models, and the Lasso algorithm is used as a meta-model for the integrated learning model to invert the LNC, and comparative analyses are performed on the two sets of data models. Parameter searching for two machine learning models SVM and RF was carried out with a grid search algorithm, and 5-fold cross-validation to improve the model's generalization ability.

Evaluation metrics: R^2, MAE, and MSE are used as evaluation metrics to assess model performance.

2.3.1. Constructing Typical VIs

In order to compare the ability of the stacking model to handle high-dimensional and geodimensional features, the study constructed spectral-stacking and VI-stacking radish LNC whole growth stage estimation models. Twenty typical VIs of LNC used in previous studies were constructed, as shown in Table 1.

Table 1. VI calculation formula.

VI	Formulae	Reference
Ratio Vegetation Index (RVI)	R_{735}/R_{720}	[35]
Normalized Difference IR Index (NDII)	$(R_{850} - R_{1650})/(R_{850} + R_{1650})$	[37]
Normalized Difference Snow Index (NDSI)	$(R_{1402} - R_{2272})/(R_{1402} + R_{2272})$	[38]
Difference Vegetation Index (DVI)	$R_{810} - R_{680}$	[39]
Water Content Index (WCI)	R_{900}/R_{970}	[40]
Water Stress Index (WSI)	R_{1600}/R_{820}	[40]
Visible Atmospheric Resistant Index (VARI)	$(R_{555} - R_{645})/(R_{555} + R_{645} - R_{469})$	[41]
Normalized Difference Vegetation Index (NDVI)	$(R_{780} - R_{550})/(R_{780} + R_{550})$	[35]

Table 1. *Cont.*

VI	Formulae	Reference
MERIS Terrestrial Chlorophyll Index (MTCI)	$(R_{750} - R_{710}) / (R_{710} - R_{680})$	[42]
Green Normalized Difference Vegetation Index (GNDVI)	$(R_{750} - R_{550}) / (R_{750} + R_{550})$	[35]
Pigment Specific Normalized Difference (PSNDc)	$(R_{800} - R_{470}) / (R_{800} + R_{470})$	[43]
Simple Ratio Index (SR1)	R_{800} / R_{550}	[40]
SR2	$R_{675} / (R_{700} * R_{650})$	[40]
SR3	$R_{672} / (R_{550} * R_{708})$	[40]
SR4	$R_{860} / (R_{550} * R_{708})$	[40]
SR5	R_{750} / R_{550}	[40]
SR6	R_{550} / R_{850}	[40]
Temperature Condition Index (TCI)	$1.2 * (R_{700} - R_{550}) - 1.5 * (R_{670} - R_{550}) * sqrt(R_{700} / R_{670})$	[43]
Modified Chlorophyll Absorption in Reflectance Index (MCARI)	$(R_{700} - R_{670}) - 0.2 * (R_{700} - R_{550}) / (R_{700} / R_{670})$	[43]
Normalized Pheophytization Index (NPQI)	$(R_{415} - R_{435}) / (R_{415} + R_{435})$	[41]

2.3.2. Model Setting

Base model: SVM allows the model to be globally optimized by creating a "spacer band" on both sides of the linear function and not calculating the loss for all samples that fall within it. That means that only the support vectors have an impact on the model, not the entire sample space. Few support vectors determine the final result with good robustness [44]. RF generates a new set of training samples to form a random forest by resampling as well as randomly extracting features, and each decision tree relies on an independently extracted set of samples to make predictions through multiple decision trees. This randomization of resampling and feature selection can effectively avoid model overfitting [45]. Ridge is actually a modified least squares estimation method to obtain a more realistic regression at the expense of losing some information and decreasing accuracy [46]. KNN takes the samples with high similarity and uses the mean of K neighbors as the prediction after mapping to n as space [47].

Meta-model: Based on traditional linear regression, Lasso achieved data downscaling and overfitting by introducing the L1 paradigm as a regularization term to constrain the model weights while minimizing the squared error loss function [48,49]. As λ increases, the greater regularization strength forces more weight coefficients to converge to zero. That means that when Lasso is used as a meta-model, the weights of the poorly performing base model can be reduced to exactly zero, while the well performing model is given higher weights.

The core principle of Lasso regression is the contraction property of the weight coefficients in the regularization process. The optimization objective function is:

$$min_w \frac{1}{2n} \| X_w - y \|_2^2 + \lambda \| w \|_1 \quad (2)$$

where X is the feature matrix, y represents the target variable, w is the weight vector, n is the number of samples, and λ is the regularization strength parameter. L1 regularization $\| w \|_1$ is used to implement the weight coefficients of the compression features.

2.4. Evaluation Indicators

The coefficient of determination (R^2), mean absolute error (MAE), and mean square error (MSE) were used to evaluate the model performance. R^2 measures how well the model fits the data, and MAE and MSE measure how well the predicted values match the true values. The calculations are as follows:

$$R^2 = 1 - \frac{\sum_{i=1}^{n} (y_i - x_i)^2}{\sum_{i=1}^{n} (y_i - \overline{y})^2} \quad (3)$$

$$\mathrm{MAE} = \frac{1}{n}\sum_{i=1}^{n}|x_i - y_i| \quad (4)$$

$$\mathrm{MSE} = \frac{1}{n}\sum_{i=1}^{n}\left(x_i - y_i\right)^2 \quad (5)$$

where y_i, x_i, and x_i are the average of the predicted, measured, and actual LNC values, and n is the number of model samples.

3. Results and Analysis

3.1. Feature Selection

Figure 4 represents the correlation of each band and typical VI with the LNC calculated using Pearson, and the red bars in Figure 4a,b are the selected important features. All leaf bands were negatively correlated with the LNC, with 136 bands and four typical VIs (VARI, SR2, SR4, TCI) reaching a significant negative correlation with correlation coefficients of less than −0.6, a relationship that was highly significant at $p < 0.001$.

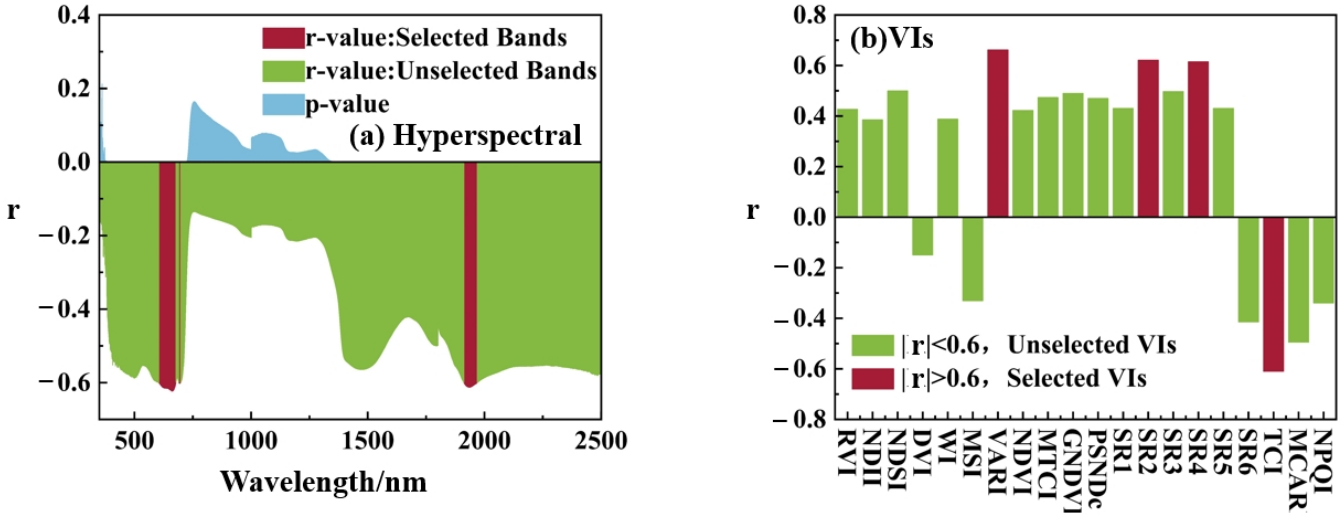


Figure 4. Correlation coefficients of different input features with the LNC. (**a**) Hyperspectral; (**b**) VIs.

The sensitive bands are concentrated around 600–700 nm as well as 1950 nm, and the four typical VIs screened have also been constructed mainly in these bands. This is due to the strong correlation between N and Chl, LNC and LCC having similar sensitive spectral regions at the leaf scale, and the fact that the absolute correlation between reflectance and N in the visible region is higher than the correlation in the infrared region, and thus exhibits relatively high absolute values near 660 nm. The bands located in the infrared region can also be used as predictive features of the LNC due to their association with the chemical bonding of N-containing compounds, a conclusion also argued by [50]. Therefore, in this study, 136 bands (high-dimensional features) as well as 4 VIs (low-dimensional features) were selected as inputs to the stacking model to construct a full-life radish LNC prediction model.

3.2. Comparative Analysis of Models

To explore stacking's ability to process data of different dimensions, the study collected in situ hyperspectral data of radish leaves at three key reproductive stages, rosette stage, fleshy root growth stage, and maturity stage, and constructed VIs for analysis and comparison. Based on the Pearson feature-analysis method to screen the sensitive features, the optimal features were used as model input parameters, and the integrated learning model was used to establish the LNC prediction model for radish during the whole reproductive stage.

The structure of the integrated learning model is shown in Figure 3. The study used six base models for 5-fold cross-validation of the training data, with each cross-validation consisting of two parts: The Training data are split into five parts, four of which are used to

train the model and the remaining one is predicted on the model trained on this part of the data to obtain Predict i. The model generated based on Training data training predicts the Testing data. By averaging the five results Predictions i is averaged as the input features of the meta-model, the Training data and Testing data of the meta-model. Overfitting is common in machine learning applications. The root cause is that the amount of training data is insufficient to support a complex model, causing the model to learn noise on the dataset, which reduces the model's generalization ability. Overfitting can be mitigated to some extent by averaging the results through 5-fold cross-validation.

Different machine learning models have different data requirements, and the four selected learning models are not necessarily applicable to LNC prediction at different scales, so the study chooses Lasso regression as the meta-model. We optimize model prediction performance and complexity by constraining the L1 paradigm of the model weight vector while minimizing the squared error loss function. That means when we increase λ, the model will tend to select fewer features, and the larger regularization strength will force the weight coefficients of the poorly performing models in the base model to converge to 0, thus filtering out the base model suitable for the dataset for stacking integration.

3.2.1. Integrated Learning Estimation of Full-Birthday LNC Based on Different Characteristics

The results of the LNC prediction model for the full-birth period with different feature inputs are shown in Figures 5 and 6 and Table 2, and the integrated learning model with high-dimensional hyperspectral data as input features achieved better prediction results where R^2 = 0.7, MAE = 0.16, MSE = 0.05, indicating that Stacking can effectively deal with the noise and outlier problems existing in high-dimensional data and improve the fitting performance. Full-band hyperspectral data are therefore more suitable for assessing vegetation traits than vegetation indices in this model, further demonstrating the ability of in situ hyperspectral data to retrieve crop nutrients. In the two stacking models constructed, some of the points of the base model lie outside the 95% prediction interval, and the predicted values of the LNC are more concentrated after stacking, indicating that the predictive performance of the model is good and robust after stacking the traditional machine learning model for stacking.

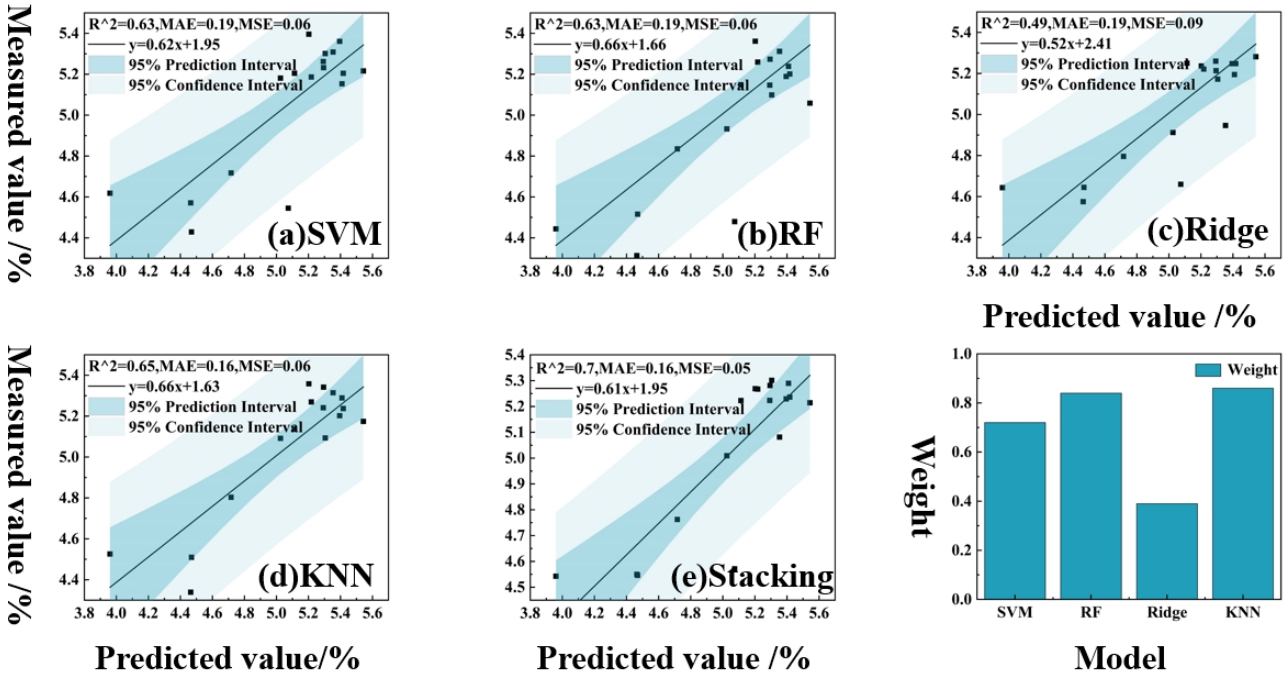


Figure 5. Hyperspectral estimation model of LNC at the whole growth stage of radish.

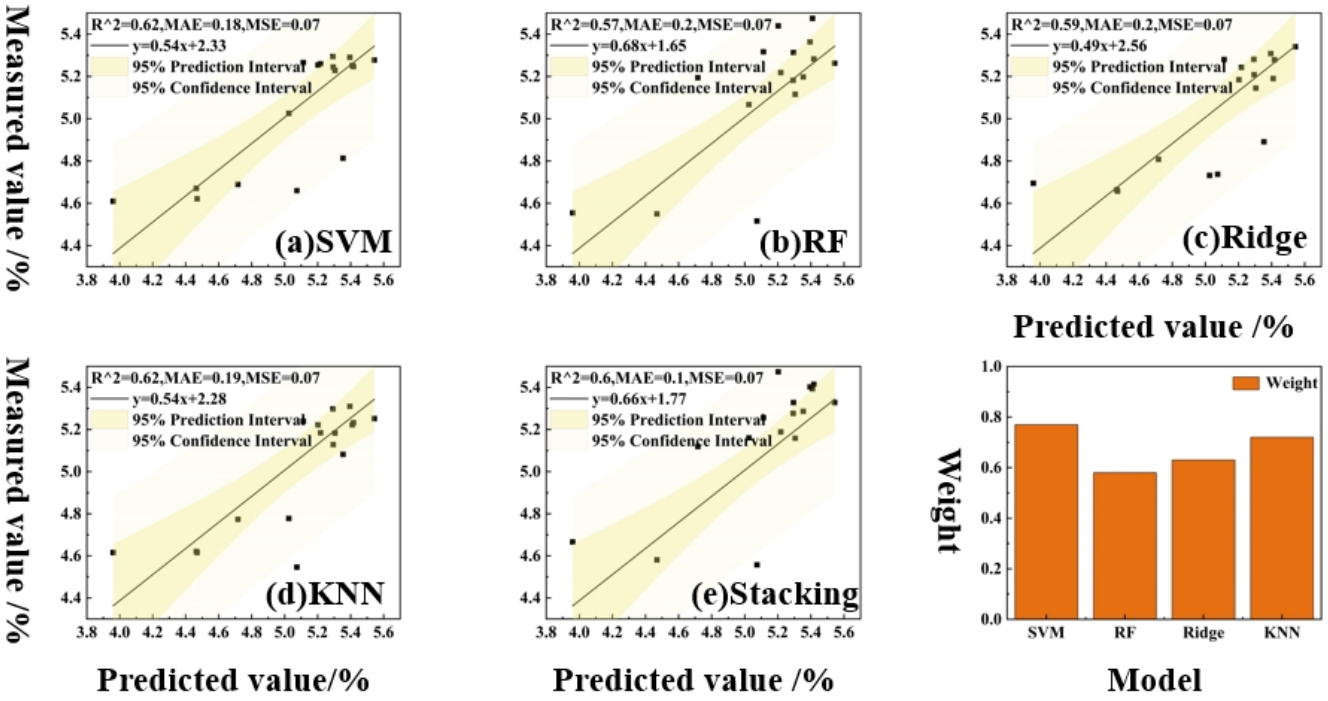


Figure 6. VI estimation model of LNC at the whole growth stage of radish.

Table 2. Evaluation index of LNC stacking prediction model at the whole growth stage of radish.

Feature Selector	Model	R^2	MAE	MSE
Hyperspectral	SVM	0.63	0.19	0.06
	RF	0.63	0.19	0.06
	Ridge	0.49	0.19	0.09
	KNN	0.65	0.16	0.06
	Stacking	0.7	0.16	0.05
VIs	SVM	0.62	0.18	0.07
	RF	0.57	0.2	0.07
	Ridge	0.59	0.2	0.07
	KNN	0.62	0.19	0.07
	Stacking	0.6	0.1	0.07

When the base model does not work well, simple stacking creates redundancy that affects the meta-modeling results. For example, for the Ridge regression model in the hyperspectral-stacking model, the study uses in situ hyperspectral data for analysis, which leads to the possible existence of anomalous spectral data, and Ridge, although it enhances the model robustness to a certain extent, still belongs to the category of linear models, which are more sensitive to the outliers, and thus when dealing with the use of spectral data for analysis less effective. This anomaly can be reduced by constructing VIs, so Ridge performs better in the VI model. The study uses the Lasso algorithm as a meta-model, and further feature selection of the base model results by introducing the L1 paradigm as a regularization term to force the unimportant feature weight coefficients to converge to zero. That is, reducing the influence of Ridge on the results of the hyperspectral model further improves the interpretability and generalization of the model. For the rest of the base models, the SVM is robust to outliers as it focuses on intervals and support vectors, and thus performs better in both models, with a higher weight in the meta-model. The RF algorithm has good generalization ability by weighted averaging the results of multiple decision trees and is more suitable for dealing with high-dimensional data, so it performs better in hyperspectral models and carries less weight in VIs.

This suggests that using Lasso regression as a meta-model can effectively filter poorly performing base models when considering inversion based on integrated learning models, thus improving prediction accuracy. The method significantly improves the accuracy and generalization of the overall model, taking full advantage of the strengths and characteristics of different models to provide more accurate predictions.

3.2.2. Validation of Two Models for LNC of Radish at Multiple Growth Stages

Figure 7 represents the modeled radish LNC remote sensing monitoring model at all different growth stages (10 sample points), where squares indicate predicted values, stars indicate the error between measured and predicted values, and the four periods represent the rosette stage (4 November 2023), the fleshy root growth stage (29 November 2023, 20 December 2023), and the maturity stage (10 January 2024). It can be seen that the sum of the absolute values of the difference between the measured and predicted values in the hyperspectral model at different growth stages was 0.98%, 1.79%, 1.43%, 1.69%, while this value was 1.44%, 1.83%, 1.58%, 1.9%, respectively, in the spectral model. Therefore, combining stacking with high-dimensional spectral data showed superior performance at different growth stages. The predicted value of radish LNC showed a tendency of decreasing and then increasing with the growth stage, which is consistent with the measured results. The hyperspectral model had the highest range of LNC predictions at the rosette stage in the range 4.98–5.48%, and the ranges 4.71–5.32% and 4.81–5.37% for the fleshy root growth period, and the range 4.55–5.19% at maturity. The VI model also had the highest range of LNC predictions at the rosette stage between 4.89 and 5.42%, and the fleshy root growth stage in the ranges 4.45–5.17% and 4.67–5.24%, respectively, and between 4.55 and 5.32% at maturity. Both models conformed to the radish growth pattern, and the overall situation was consistent with the experimental results in the field. This result can provide a reference for radish LNC monitoring, which is very important for guiding the precise fertilization of radish in the field.

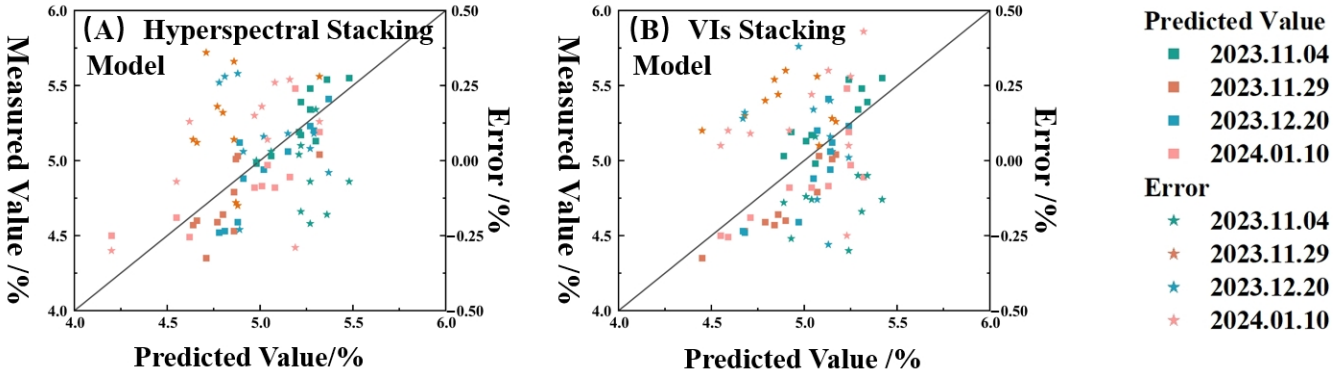


Figure 7. Validation of LNC in radish at different growth stages. (**A**) Hyperspectral stacking model; (**B**) VI stacking model.

4. Discussion

Crop spectral response can sense subtle changes in chemical and physical parameters, providing a broad characterization space for realizing real-time and effective nutrient monitoring and diagnostic information. However, reflectance data from neighboring bands are highly correlated, and data from thousands of spectral bands contain a large amount of redundant information, resulting in a "dimensional catastrophe", which leads to increased complexity and risk of overfitting in prediction models [51]. During the acquisition process, spectral data will contain a large amount of noise due to the influence of the instrument and the measurement environment; therefore, when constructing a hyperspectral prediction model, it is necessary to consider how to reduce the data dimensionality through feature screening and eliminate redundant and noisy information to improve the model performance [52].

In this study, in situ hyperspectral data of radish leaves were collected and 20 typical VIs were constructed, and the LNC response characteristics of different data were analyzed using the Pearson algorithm, and features above $|r| > 0.6$ were selected as input variables. The hyperspectral sensitive bands are mainly concentrated around 600–700 nm as well as 1950 nm due to the correlation between N and Chl. The sensitive regions for LNC and LCC were similar for different crop hyperspectral data, with higher absolute values of correlation coefficients for spectra in the visible region than in the infrared region, and relatively high absolute values of correlation coefficients near 660 nm. The band near 1950 nm is associated with chemical bonding of N-containing compounds and can also be used as a predictor to characterize the LNC, a finding consistent with the analysis of [51].

In this study, four models, SVM, RF, Ridge, and KNN, were selected as base models, and Lasso regression was used as a meta-model to construct the stacking-integrated learning regression model. All four base models achieved better results in the prediction of LNC in different crops [53,54], but some of the base models were not as effective in the prediction of LNC in radish during the whole life span. In the hyperspectral-stacking model, the base model Ridge is less effective; this is due to the presence of outliers in the spectral data due to noise, environment, and other effects; the model is more sensitive to the outliers, resulting in poor prediction accuracy; in future research, some spectral data could undergo preprocessing, such as the fractional order of change (FOD), and the wavelet change (CWT) [46]. However, the poorer performing models were compressed with weights by the meta-model Lasso, which reduced the impact of the overall accuracy of this model, further explaining the generalization ability of the integrated learning framework proposed in this study. Since different machine learning models have different data requirements, the framework can take full advantage of the strengths and characteristics of different models to provide more accurate prediction results, and thus can be validated by introducing different crop data in future studies.

The study used two dimensions of features as model inputs (hyperspectral and VIs), and the results showed that high-latitude hyperspectral data combined with stacking achieved superior results in terms of radish LNC monitoring capability throughout the whole life cycle, and this result was also validated at different growth stages of radish. This also indicates that the model is more suitable for dealing with high-dimensional features and large-scale datasets [55]. However, due to the limited conditions, the data used in the study are all from one year, so it is necessary to introduce multi-year data to validate and improve the reliability of the model in future studies.

5. Conclusions

Hyperspectral remote sensing technology has been improving and maturing in crop nutrient monitoring and prediction and diagnostic decision-making, but the prediction models for different crops are not universal. In this study, we collected hyperspectral reflectance and field sample nitrogen data of white radish over multiple growth stages. We used four machine learning models (SVM, RF, Ridge, and KNN) as base models in the first-layer architecture and Lasso algorithm as a meta-model stacking framework in the second-layer architecture for radish LNC prediction. By applying the Pearson feature-selection method to calculate the importance of spectral feature variables and VIs of the LNC response, the radish leaf feature bands were mainly concentrated at 600–700 nm as well as 1950 nm. After inputting the characteristic bands and typical VIs into this stacking framework, the accuracy of predicting the LNC of radish during all the reproductive stages by high-dimensional hyperspectral was higher, and this finding was also verified in different growth stages. Lasso reduces the weight of underperforming base models, effectively improving the overall accuracy of the algorithm. The framework showed good results in predicting the LNC of radish at different growth stages, and the method can also provide methodological references and ideas for spectroscopic monitoring of physiological and biochemical indicators in other crops.

Author Contributions: Conceptualization, X.X., L.G. and W.W.; writing—original draft preparation, Y.Z. and G.Y.; writing—review and editing, Y.L., Y.M., X.J. and H.X. All authors have read and agreed to the published version of the manuscript.

Funding: This research was funded by Yunnan Province Major Science and Technology Special Project (202202AE090013-2) and National Modern Agricultural Industry Technology System Grant (CARS-03).

Data Availability Statement: The data that support the findings of this study are available from the corresponding author, upon reasonable request.

Conflicts of Interest: All authors disclosed no relevant relationships.

References

1. Fu, Y.; Yang, G.; Pu, R.; Li, Z.; Li, H.; Xu, X.; Song, X.; Yang, X.; Zhao, C. An Overview of Crop Nitrogen Status Assessment Using Hyperspectral Remote Sensing: Current Status and Perspectives. *Eur. J. Agron.* **2021**, *124*, 126241. [CrossRef]
2. Tei, F.; De Neve, S.; de Haan, J.; Kristensen, H.L. Nitrogen Management of Vegetable Crops. *Agric. Water Manag.* **2020**, *240*, 106316. [CrossRef]
3. Lemaire, G.; Jeuffroy, M.-H.; Gastal, F. Diagnosis Tool for Plant and Crop N Status in Vegetative Stage: Theory and Practices for Crop N Management. *Eur. J. Agron.* **2008**, *28*, 614–624. [CrossRef]
4. Berger, K.; Verrelst, J.; Féret, J.-B.; Wang, Z.; Wocher, M.; Strathmann, M.; Danner, M.; Mauser, W.; Hank, T. Crop Nitrogen Monitoring: Recent Progress and Principal Developments in the Context of Imaging Spectroscopy Missions. *Remote Sens. Environ.* **2020**, *242*, 111758. [CrossRef]
5. Thompson, R.B.; Martínez-Gaitan, C.; Gallardo, M.; Giménez, C.; Fernández, M.D. Identification of Irrigation and N Management Practices That Contribute to Nitrate Leaching Loss from an Intensive Vegetable Production System by Use of a Comprehensive Survey. *Agric. Water Manag.* **2007**, *89*, 261–274. [CrossRef]
6. Vaziritabar, Y.; Frei, M.; Yan, F.; Vaziritabar, Y.; Honermeier, B. Enhancing Nitrogen Use Efficiency and Plant Productivity in Long-Term Precrop/Crop Rotation and Fertilization Management. *Field Crops Res.* **2024**, *306*, 109210. [CrossRef]
7. Zhou, X.; Huang, W.; Kong, W.; Ye, H.; Luo, J.; Chen, P. Remote Estimation of Canopy Nitrogen Content in Winter Wheat Using Airborne Hyperspectral Reflectance Measurements. *Adv. Space Res.* **2016**, *58*, 1627–1637. [CrossRef]
8. Wei, C.; Qin, H.; Ji, J.; Wang, W.; Hua, Y.; Yao, Y.; Yu, W.; Hou, H.; Zhou, W. Estimating Aboveground Biomass of Urban Trees Based on ICESat-2 LiDAR and Zhuhai-1 Hyperspectral Data. *Phys. Chem. Earth Parts A/B/C* **2024**, *135*, 103605. [CrossRef]
9. Jiang, X.; Zhen, J.; Miao, J.; Zhao, D.; Wang, J.; Jia, S. Assessing Mangrove Leaf Traits under Different Pest and Disease Severity with Hyperspectral Imaging Spectroscopy. *Ecol. Indic.* **2021**, *129*, 107901. [CrossRef]
10. Guo, Y.; Xiao, Y.; Hao, F.; Zhang, X.; Chen, J.; de Beurs, K.; He, Y.; Fu, Y.H. Comparison of Different Machine Learning Algorithms for Predicting Maize Grain Yield Using UAV-Based Hyperspectral Images. *Int. J. Appl. Earth Obs. Geoinf.* **2023**, *124*, 103528. [CrossRef]
11. Du, R.; Chen, J.; Xiang, Y.; Zhang, Z.; Yang, N.; Yang, X.; Tang, Z.; Wang, H.; Wang, X.; Shi, H.; et al. Incremental Learning for Crop Growth Parameters Estimation and Nitrogen Diagnosis from Hyperspectral Data. *Comput. Electron. Agric.* **2023**, *215*, 108356. [CrossRef]
12. Feng, W.; Zhang, H.-Y.; Zhang, Y.-S.; Qi, S.-L.; Heng, Y.-R.; Guo, B.-B.; Ma, D.-Y.; Guo, T.-C. Remote Detection of Canopy Leaf Nitrogen Concentration in Winter Wheat by Using Water Resistance Vegetation Indices from In-Situ Hyperspectral Data. *Field Crops Res.* **2016**, *198*, 238–246. [CrossRef]
13. Wang, W.; Yao, X.; Yao, X.; Tian, Y.; Liu, X.; Ni, J.; Cao, W.; Zhu, Y. Estimating Leaf Nitrogen Concentration with Three-Band Vegetation Indices in Rice and Wheat. *Field Crops Res.* **2012**, *129*, 90–98. [CrossRef]
14. Lu, J.; Cheng, D.; Geng, C.; Zhang, Z.; Xiang, Y.; Hu, T. Combining Plant Height, Canopy Coverage and Vegetation Index from UAV-Based RGB Images to Estimate Leaf Nitrogen Concentration of Summer Maize. *Biosyst. Eng.* **2021**, *202*, 42–54. [CrossRef]
15. Yang, Z.; Tian, J.; Feng, K.; Gong, X.; Liu, J. Application of a Hyperspectral Imaging System to Quantify Leaf-Scale Chlorophyll, Nitrogen and Chlorophyll Fluorescence Parameters in Grapevine. *Plant Physiol. Biochem.* **2021**, *166*, 723–737. [CrossRef] [PubMed]
16. Li, B.; Xu, X.; Zhang, L.; Han, J.; Bian, C.; Li, G.; Liu, J.; Jin, L. Above-Ground Biomass Estimation and Yield Prediction in Potato by Using UAV-Based RGB and Hyperspectral Imaging. *ISPRS J. Photogramm. Remote Sens.* **2020**, *162*, 161–172. [CrossRef]
17. Shi, S.; Xu, L.; Gong, W.; Chen, B.; Chen, B.; Qu, F.; Tang, X.; Sun, J.; Yang, J. A Convolution Neural Network for Forest Leaf Chlorophyll and Carotenoid Estimation Using Hyperspectral Reflectance. *Int. J. Appl. Earth Obs. Geoinf.* **2022**, *108*, 102719. [CrossRef]
18. Tan, K.; Wang, S.; Song, Y.; Liu, Y.; Gong, Z. Estimating Nitrogen Status of Rice Canopy Using Hyperspectral Reflectance Combined with BPSO-SVR in Cold Region. *Chemom. Intell. Lab. Syst.* **2018**, *172*, 68–79. [CrossRef]
19. Thorp, K.R.; Wang, G.; Bronson, K.F.; Badaruddin, M.; Mon, J. Hyperspectral Data Mining to Identify Relevant Canopy Spectral Features for Estimating Durum Wheat Growth, Nitrogen Status, and Grain Yield. *Comput. Electron. Agric.* **2017**, *136*, 1–12. [CrossRef]

20. Guo, P.-T.; Li, M.-F.; Luo, W.; Cha, Z.-Z. Estimation of Foliar Nitrogen of Rubber Trees Using Hyperspectral Reflectance with Feature Bands. *Infrared Phys. Technol.* **2019**, *102*, 103021. [CrossRef]
21. Vaddi, R.; Phaneendra Kumar, B.L.N.; Manoharan, P.; Agilandeeswari, L.; Sangeetha, V. Strategies for Dimensionality Reduction in Hyperspectral Remote Sensing: A Comprehensive Overview. *Egypt. J. Remote Sens. Space Sci.* **2024**, *27*, 82–92. [CrossRef]
22. Jiachen, H.; Jing, H.; Gang, L.; Weile, L.; Zhe, L.; Zhi, L. Inversion Analysis of Soil Nitrogen Content Using Hyperspectral Images with Different Preprocessing Methods. *Ecol. Inform.* **2023**, *78*, 102381. [CrossRef]
23. Yu, F.; Bai, J.; Jin, Z.; Guo, Z.; Yang, J.; Chen, C. Combining the Critical Nitrogen Concentration and Machine Learning Algorithms to Estimate Nitrogen Deficiency in Rice from UAV Hyperspectral Data. *J. Integr. Agric.* **2023**, *22*, 1216–1229. [CrossRef]
24. Guo, B.-B.; Feng, Y.-L.; Ma, C.; Zhang, J.; Song, X.; Wang, M.-Y.; Sheng, D.-H.; Feng, W.; Jiao, N. Suitability of Different Multivariate Analysis Methods for Monitoring Leaf N Accumulation in Winter Wheat Using in Situ Hyperspectral Data. *Comput. Electron. Agric.* **2022**, *198*, 107115. [CrossRef]
25. Xue, L.; Yang, L. Deriving Leaf Chlorophyll Content of Green-Leafy Vegetables from Hyperspectral Reflectance. *ISPRS J. Photogramm. Remote Sens.* **2009**, *64*, 97–106. [CrossRef]
26. Li, J.; Ge, Y.; Puntel, L.A.; Heeren, D.M.; Bai, G.; Balboa, G.R.; Gamon, J.A.; Arkebauer, T.J.; Shi, Y. Integrating UAV Hyperspectral Data and Radiative Transfer Model Simulation to Quantitatively Estimate Maize Leaf and Canopy Nitrogen Content. *Int. J. Appl. Earth Obs. Geoinf.* **2024**, *129*, 103817. [CrossRef]
27. Li, L.; Jákli, B.; Lu, P.; Ren, T.; Ming, J.; Liu, S.; Wang, S.; Lu, J. Assessing Leaf Nitrogen Concentration of Winter Oilseed Rape with Canopy Hyperspectral Technique Considering a Non-Uniform Vertical Nitrogen Distribution. *Ind. Crops Prod.* **2018**, *116*, 1–14. [CrossRef]
28. He, Y.; Zhang, H.; Dong, Y.; Wang, C.; Ma, P. Residential Net Load Interval Prediction Based on Stacking Ensemble Learning. *Energy* **2024**, *296*, 131134. [CrossRef]
29. Hao, X.; Chen, Z.; Yi, S.; Liu, J. Application of Improved Stacking Ensemble Learning in NIR Spectral Modeling of Corn Seed Germination Rate. *Chemom. Intell. Lab. Syst.* **2023**, *243*, 105020. [CrossRef]
30. Xiao, B.; Li, S.; Dou, S.; He, H.; Fu, B.; Zhang, T.; Sun, W.; Yang, Y.; Xiong, Y.; Shi, J.; et al. Comparison of Leaf Chlorophyll Content Retrieval Performance of Citrus Using FOD and CWT Methods with Field-Based Full-Spectrum Hyperspectral Reflectance Data. *Comput. Electron. Agric.* **2024**, *217*, 108559. [CrossRef]
31. Huang, X.; Guan, H.; Bo, L.; Xu, Z.; Mao, X. Hyperspectral Proximal Sensing of Leaf Chlorophyll Content of Spring Maize Based on a Hybrid of Physically Based Modelling and Ensemble Stacking. *Comput. Electron. Agric.* **2023**, *208*, 107745. [CrossRef]
32. Xiong, W.; Xiao, L.; Han, D.; Yue, W. A Prediction Model for Water Absorption in Sublayers Based on Stacking Ensemble Learning Method. *Geoenergy Sci. Eng.* **2024**, *239*, 212896. [CrossRef]
33. Yu, F.-W.; Ho, W.-T.; Wong, C.-F.J. Predicting and Decarbonizing Carbon Emissions from Building Energy Use in Hong Kong: A LASSO Regression Approach. *Energy Sustain. Dev.* **2024**, *78*, 101374. [CrossRef]
34. Yu, W.; Li, J.; Li, H.; Shi, F.; Wu, G. Investigation into Relationships between Grain Size Distribution Characteristics and Mechanical Properties in Large-Scaled Complex Titanium Alloy Castings Utilizing LASSO Regression. *J. Alloys Compd.* **2024**, *977*, 173409. [CrossRef]
35. Liu, Y.; Fan, Y.; Feng, H.; Chen, R.; Bian, M.; Ma, Y.; Yue, J.; Yang, G. Estimating Potato Above-Ground Biomass Based on Vegetation Indices and Texture Features Constructed from Sensitive Bands of UAV Hyperspectral Imagery. *Comput. Electron. Agric.* **2024**, *220*, 108918. [CrossRef]
36. Xu, T.; Wang, F.; Shi, Z.; Xie, L.; Yao, X. Dynamic Estimation of Rice Aboveground Biomass Based on Spectral and Spatial Information Extracted from Hyperspectral Remote Sensing Images at Different Combinations of Growth Stages. *ISPRS J. Photogramm. Remote Sens.* **2023**, *202*, 169–183. [CrossRef]
37. Joiner, J.; Yoshida, Y.; Anderson, M.; Holmes, T.; Hain, C.; Reichle, R.; Koster, R.; Middleton, E.; Zeng, F.-W. Global Relationships among Traditional Reflectance Vegetation Indices (NDVI and NDII), Evapotranspiration (ET), and Soil Moisture Variability on Weekly Timescales. *Remote Sens. Environ.* **2018**, *219*, 339–352. [CrossRef]
38. Zhang, S.; Huang, X.; Ma, L.; Dashzevegd, G.; Ariunaa, M.; Bao, G.; Tong, S.; Bao, Y.; Dorjsuren, A.; Enkhnasan, D. Response of Spectral Vegetation Indices to *Erannis Jacobsoni* Djak. Damage in Larch Forests. *Ecol. Inform.* **2024**, *81*, 102605. [CrossRef]
39. Wei, Y.; Lu, M.; Yu, Q.; Li, W.; Wang, C.; Tang, H.; Wu, W. The Normalized Difference Yellow Vegetation Index (NDYVI): A New Index for Crop Identification by Using GaoFen-6 WFV Data. *Comput. Electron. Agric.* **2024**, *226*, 109417. [CrossRef]
40. Minaei, S.; Soltanikazemi, M.; Shafizadeh-Moghadam, H.; Mahdavian, A. Field-Scale Estimation of Sugarcane Leaf Nitrogen Content Using Vegetation Indices and Spectral Bands of Sentinel-2: Application of Random Forest and Support Vector Regression. *Comput. Electron. Agric.* **2022**, *200*, 107130. [CrossRef]
41. Wang, D.; Li, R.; Liu, T.; Liu, S.; Sun, C.; Guo, W. Combining Vegetation, Color, and Texture Indices with Hyperspectral Parameters Using Machine-Learning Methods to Estimate Nitrogen Concentration in Rice Stems and Leaves. *Field Crop. Res.* **2023**, *304*, 109175. [CrossRef]
42. Zhu, X.; Li, Q.; Guo, C. Evaluation of the Monitoring Capability of Various Vegetation Indices and Mainstream Satellite Band Settings for Grassland Drought. *Ecol. Inform.* **2024**, *82*, 102717. [CrossRef]
43. Thinley, J.; Pickering, C.; Ndehedehe, C. Using Vegetation and Chlorophyll Indices to Model above Ground Biomass over Time in an Urban Arboretum in Subtropical Queensland. *Remote Sens. Appl. Soc. Environ.* **2024**, *34*, 101202. [CrossRef]

44. Lai, Z.; Liang, G.; Zhou, J.; Kong, H.; Lu, Y. A Joint Learning Framework for Optimal Feature Extraction and Multi-Class SVM ☆. *Inf. Sci.* **2024**, *671*, 120656. [CrossRef]
45. Feng, Z.; Guan, H.; Yang, T.; He, L.; Duan, J.; Song, L.; Wang, C.; Feng, W. Estimating the Canopy Chlorophyll Content of Winter Wheat under Nitrogen Deficiency and Powdery Mildew Stress Using Machine Learning. *Comput. Electron. Agric.* **2023**, *211*, 107989. [CrossRef]
46. Huang, H.; Fang, Z.; Xu, Y.; Lu, G.; Feng, C.; Zeng, M.; Tian, J.; Ping, Y.; Han, Z.; Zhao, Z. Stacking and Ridge Regression-Based Spectral Ensemble Preprocessing Method and Its Application in near-Infrared Spectral Analysis. *Talanta* **2024**, *276*, 126242. [CrossRef] [PubMed]
47. Sumayli, A. Development of Advanced Machine Learning Models for Optimization of Methyl Ester Biofuel Production from Papaya Oil: Gaussian Process Regression (GPR), Multilayer Perceptron (MLP), and K-Nearest Neighbor (KNN) Regression Models. *Arab. J. Chem.* **2023**, *16*, 104833. [CrossRef]
48. Saperas-Riera, J.; Mateu-Figueras, G.; Martin-Fernandez, J.A. Lasso Regression Method for a Compositional Covariate Regularised by the Norm L^1 Pairwise Logratio. *J. Geochem. Explor.* **2023**, *255*, 107327. [CrossRef]
49. Shafiee, S.; Lied, L.M.; Burud, I.; Dieseth, J.A.; Alsheikh, M.; Lillemo, M. Sequential Forward Selection and Support Vector Regression in Comparison to LASSO Regression for Spring Wheat Yield Prediction Based on UAV Imagery. *Comput. Electron. Agric.* **2021**, *183*, 106036. [CrossRef]
50. Yoder, B.J.; Pettigrew-Crosby, R.E. Predicting Nitrogen and Chlorophyll Content and Concentrations from Reflectance Spectra (400–2500 Nm) at Leaf and Canopy Scales. *Remote Sens. Environ.* **1995**, *53*, 199–211. [CrossRef]
51. Chen, S.; Hu, T.; Luo, L.; He, Q.; Zhang, S.; Li, M.; Cui, X.; Li, H. Rapid Estimation of Leaf Nitrogen Content in Apple-Trees Based on Canopy Hyperspectral Reflectance Using Multivariate Methods. *Infrared Phys. Technol.* **2020**, *111*, 103542. [CrossRef]
52. Cao, C.; Wang, T.; Gao, M.; Li, Y.; Li, D.; Zhang, H. Hyperspectral Inversion of Nitrogen Content in Maize Leaves Based on Different Dimensionality Reduction Algorithms. *Comput. Electron. Agric.* **2021**, *190*, 106461. [CrossRef]
53. Wang, L.; Zhou, X.; Zhu, X.; Guo, W. Estimation of Leaf Nitrogen Concentration in Wheat Using the MK-SVR Algorithm and Satellite Remote Sensing Data. *Comput. Electron. Agric.* **2017**, *140*, 327–337. [CrossRef]
54. Shu, M.; Zhu, J.; Yang, X.; Gu, X.; Li, B.; Ma, Y. A Spectral Decomposition Method for Estimating the Leaf Nitrogen Status of Maize by UAV-Based Hyperspectral Imaging. *Comput. Electron. Agric.* **2023**, *212*, 108100. [CrossRef]
55. Tao, S.; Zhang, X.; Feng, R.; Qi, W.; Wang, Y.; Shrestha, B. Retrieving Soil Moisture from Grape Growing Areas Using Multi-Feature and Stacking-Based Ensemble Learning Modeling. *Comput. Electron. Agric.* **2023**, *204*, 107537. [CrossRef]

Disclaimer/Publisher's Note: The statements, opinions and data contained in all publications are solely those of the individual author(s) and contributor(s) and not of MDPI and/or the editor(s). MDPI and/or the editor(s) disclaim responsibility for any injury to people or property resulting from any ideas, methods, instructions or products referred to in the content.